# Facile Preparation of Mesoporous Titanium Nitride Microspheres for Electrochemical Energy Storage

**Shanmu Dong,[†,‡] Xiao Chen,[†,‡] Lin Gu,[§] Xinhong Zhou,[∥] Hongxia Xu,[‡] Haibo Wang,[‡] Zhihong Liu,[‡] Pengxian Han,[‡] Jianhua Yao,[‡] Li Wang,[‡] Guanglei Cui,[*,‡] and Liquan Chen[‡,⊥]**

Qingdao Institute of Bioenergy and Bioprocess Technology, Chinese Academy of Sciences, Qingdao 266101, P. R. China, WPI Advanced Institute for Materials Research, Tohoku University, Sendai 9808577, Japan, Qingdao University of Science and Technology, Qingdao 266101, P. R. China, and Institute of Physics, Chinese Academy of Sciences, Beijing 100080, China

**ABSTRACT** In this study, mesoporous TiN spheres with tunable diameter have been fabricated via a facile template-free strategy. Under ammonia atmosphere, mesoporous $TiO_2$ spheres are directly converted into mesoporous TiN spheres with the addition of cyanamide to retain the original morphology. The electrochemical performance of the resultant mesoporous TiN spheres demonstrates that this material can be a promising electrode material for nonaqueous supercapacitors with high energy densities.

**KEYWORDS:** titanium nitride • mesoporous spheres • cyanamide • template-free method • supercapacitors • electrochemical performance

## INTRODUCTION

Titanium nitride (TiN) has drawn considerable attention for its interesting properties and various applications (1), such as abrasives and protective coating materials (2). Recent reports have found its potential use as catalyst (3−6), sensors for electroanalysis (7−9), supercapacitors (10), and also a conductive additive for lithium-ion batteries with minor capacity (1, 11). During the past decades, substantial researches have been carried out for the synthesis of materials with porous nanostructures beneficial for energy storage applications (12−19), as these materials possess high surface/volume ratio, good accessibility of the pores, and a short distance of ion diffusion or mass transport. Therefore, it is reasonably expected that a mesostructure of TiN can be potential for enhancing its electrochemical performance for lithium batteries and supercapacitor applications.

TiN nanoparticles are often prepared from titanium oxide using nitrogen sources (such as ammonia or nitrogen) at high temperature (20−27). However, it is challenging to prepare mesoporous structure, because the collapse of the nanopores during conversion and recrystallization severely hinder the formation of mesoporous TiN (28). To address this issue, the general synthetic strategies have mostly relied on the use of multiple templates (28−33). Two recently reported procedures intended for preparation mesoporous TiN deserve highlighting: (1) the use of SBA-15 and graphitic carbon nitride as sacrificial templates to fabricate 2D hexagonal mesoporous TiN/C composites (28), (2) the use of hollow $Zn_2TiO_4$ spheres formed by nebulization as an in situ templating to prepare hollow TiN mesoporous spheres (33). However, these approaches substantially require a tedious and time-consuming process of template formation and the necessity of template removal. Therefore, it is urgent to explore new template-free synthetic methods for preparing mesoporous nanostructure of TiN.

Herein, we reported a facile route to directly converted $TiO_2$ mesoporous spheres into TiN mesoporous spheres under ammonia atmosphere using cyanamide to retain the morphology. In this approach, cyanamide plays a significant role in the procedure of ammonia reduction. First, cyanamide confines the aggregate of spheres at high temperature, prevents the nanopores structure from collapse during recrystallization (4), and finally thermally decomposes without additional purification. Second, cyanamide also serves as an excess of nitrogen source to promote the nitrogenization reaction during decomposition (21, 31). Therefore, TiN can be obtained with well-maintained mesoporous spheres structure.

In addition, mesoporous TiN spheres offer an electronic conducting framework which can be expected to be an effective and fast charge-separation network desirable for the electrochemical energy storage application (34, 35). A highly effective electronic conducting network is expected to ensure a rapid electronic diffusion while the mesoporous structure can be favorable for accessible diffusion of electrolyte. Therefore, in the present study, the electrochemical

* Corresponding author. E-mail: cuigl@qibebt.ac.cn.
Received for review October 3, 2010 and accepted November 29, 2010
† These authors contributed equally to this work.
‡ Qingdao Institute of Bioenergy and Bioprocess Technology, Chinese Academy of Sciences.
§ Tohoku University.
∥ Qingdao University of Science and Technology.
⊥ Institute of Physics, Chinese Academy of Sciences.
DOI: 10.1021/am100951h

**Table 1. Composition of the Solutions for the Synthesis of Titanium Glycolate Spheres in Step One**

| materials | tetrabutoxytitanium (mL) | ethylene glycol (mL) | acetone (mL) | $H_2O$ (mL) | diameter range (nm) |
|---|---|---|---|---|---|
| TiN-1 | 2 | 50 | 170 | 30 | 50−100 |
| TiN-2 | 2 | 50 | 170 | 2.7 | 200−300 |
| TiN-3 | 2 | 50 | 170 | 0.5 | 600−800 |

performance of mesoporous TiN spheres for nonaqueous symmetric supercapacitor was also explored.

## EXPERIMENTAL SECTION

**Synthesis of Mesoporous $TiO_2$ Spheres.** All chemicals were used as received without further purification. Mesoporous $TiO_2$ spheres were prepared as described by Zhong and co-workers with minor revision (36). In the first step, titanium glycolate precursor spheres were synthesized. The exact composition of the used precursor solutions are given in Table 1. In the second step, the titanium glycolate is refluxed with 20 mL of water at 80 °C, and titanium glycolate reacts with water to form the nanoporous $TiO_2$. After refluxing for 3 h, the white precipitate was obtained by centrifugation, followed by washing with water five times and subsequently drying at 50 °C for further usage.

**Preparation of Mesoporous TiN Spheres.** The mesoporous titanium nitride spheres were prepared by using the above-described mesoporous $TiO_2$ spheres and cyanamide. In a typical synthesis experiment, 120 mg of the $TiO_2$ powder was mixed with 95 mg of cyanamide ($NH_2CN$, Aldrich) dissolved in 5 mL of absolute ethanol. The mixture was magnetically stirred for 2 h and dried at 80 °C to get a homogeneous bulk. Three $TiO_2$/cyanamide composite was then heated to 800 °C under ammonia for 1 h with a progressive, slow heating ramp (room temperature to 300 °C, 5 °C $min^{-1}$; 300 to 700 °C, 2 °C $min^{-1}$; 700 to 800 °C, 1 °C $min^{-1}$). After being cooled to room temperature, mesoporous TiN spheres were finally obtained as the resultant black powders.

**Characterization.** X-ray diffraction (XRD) patterns were recorded with a Bruker-AXS Microdiffractometer (D8 ADVANCE) using Cu Ka radiation ($\lambda$ = 1.5406 Å) from 30 to 80° at a scanning speed of 0.33° $min^{-1}$. Elemental analysis was performed using a Flash EA 1112 CHNS/O elemental analyzer from Thermo Scientific and ICP measurements were carried out by terracon GmbH, Juterbog, Germany. Morphological information was attained from field-emission scanning electron microscopy (FESEM, HITACHI S-4800). High-resolution transmission electron microscopy (HRTEM) was performed using a JEOL 4000EX transmission electron microscopy (JEOL, Tokyo, Japan) operated at 400 keV. $N_2$ adsorption- desorption measurements were carried out at 77 K using a Quantachrome Autosorb gas-sorption system. Brunauer−Emmett−Teller (BET) and Barrett−Joyner−Halenda (BJH) models were used to determine the specific surface areas and the pore sizes of the samples, respectively. Before the measurements, the samples were degassed at 200 °C under a vacuum for at least one night.

Two-electrode Swagelok-type system was employed to study the electrochemical performance of the mesoporous TiN spheres. The electrode materials were prepared by mixing the active nitride material with 5% super P and 10 wt % PTFE binders. The samples were then cut into plates of 0.5 cm × 0.5 cm and pasted on a stainless steel current-collector (with the thickness of 150 $\mu$m) under a pressure of 15 MPa. A capacitor cell was fabricated with two electrodes (typically 0.5 mg active material of each electrode) separated by a glass-fiber separator soaked in 1 M $LiPF_6$ (EC:DEC = 1:1). The electrochemical properties of the electrodes were evaluated by cyclic voltammetry (CV) using a CHI 440A instrument (CHI Instrument Inc.) and galvanostatic charge/discharge measurements conducted with a charge−discharge tester (LAND).

## RESULTS AND DISCUSSION

As a main precursor of mesoporous TiN spheres, mesoporous $TiO_2$ spheres were fabricated by a facile aqueous route reported by Zhong and co-workers (36). As shown in scanning electron microscopy (SEM) and transmission electron microscopy (TEM) images a, c, and e in Figure 1, the mesoporous $TiO_2$ spheres consist of interconnected nanoparticles 10−20 nm in size. These results are consistent with the morphology of previous report (36).

For the preparation of mesoporous TiN spheres, as shown in Scheme 1, as-prepared $TiO_2$ spheres were immersed with cyanamide dissolved in absolute ethanol. Cyanamide could penetrate through the pores and enter into the mesoprous spheres. The $TiO_2$/cyanamide composites were subsequently heated to 800 °C under ammonia atmosphere. Antonietti et al. have reported the mechanism of cyanamide severing as nanoconfinement in the process of preparing nanoparticles (31, 37) and porous materials (28). During the thermal treatment, cyanamide was condensed into carbon nitride (occurring at 550 °C) as a confining matrix. When the temperature was higher than 650 °C, carbon nitride decomposition occurred and the minor amount of carbon residue could also serve as a confinement matrix. Finally, the metal oxide spheres confined in the matrix was consequently converted into the nitride with the morphology well preserved. In a control experiment, without the addition of cyanamide (as shown in Figure S1 in the Supporting Information), microspheres aggregated together with a smooth surface and totally lost their mesoporous structure.

By changing the amount of water in the process of preparing titanium glycolate spheres, we can tune the diameters of mesoporous spheres from 100 to 800 nm. It is assumed that increasing amount of water will speed up the hydrolysis rate of precursor. Therefore, the nucleation reaction can quickly reach equilibrium to prevent the sphere size from growing larger (38). Three kinds of mesoporous spheres with different diameter range (50−100, 200−300, and 600−800 nm) were prepared and denoted hereafter as TiN-1, TiN-2, and TiN-3, respectively (Figure 1b, d, f).

The successful preparation of mesoporous TiN spheres is confirmed by electron microscopy. The SEM images (Figure 1) show that the size and morphology are consistent with the mesoporous $TiO_2$ spheres, which indicates that $TiO_2$ spheres with different diameter range have been successfully transformed into TiN without aggregation or collapse of pores. SEM images at lower magnification furthermore prove the homogeneity of the TiN samples (see Figure S2 in the Supporting Information). More detailed information is shown in the High resolution TEM (HRTEM) images (Figure 2). TiN spheres consist of mesoporous structure with pore diameters of several nanometers. High-resolution TEM image confirms that the polycrystalline characteristic of the mesoporous TiN spheres.

Combined measurements using inductively coupled plasma and elemental analysis are applied to investigate

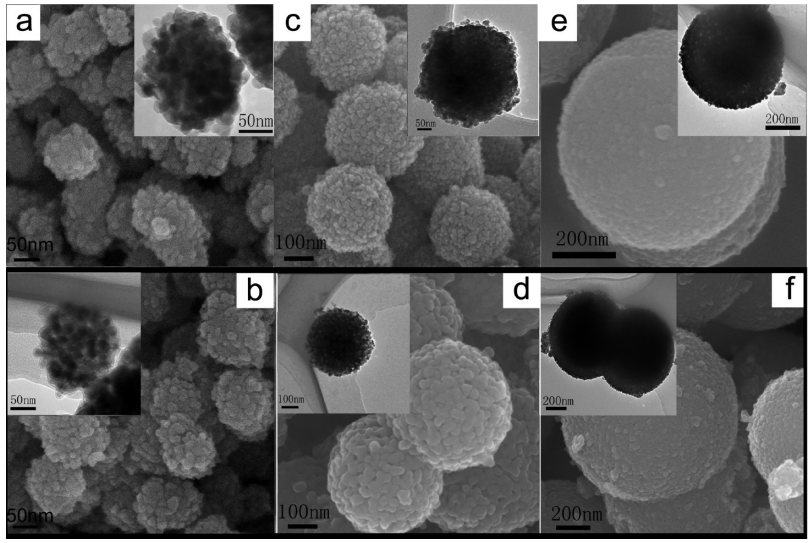


FIGURE 1. SEM images and TEM images (insert image) of mesoporous $TiO_2$ spheres with diameter range of (a) 50−100, (c) 200−300, and (e) 600−800 nm; SEM image and TEM image (insert image) of the mesoporous TiN spheres with diameter range of (b) 50−100, (d) 200−300, (f) 600−800 nm.

Scheme 1. Schematic Illustration for the Preparation of Mesoporous TiN Spheres

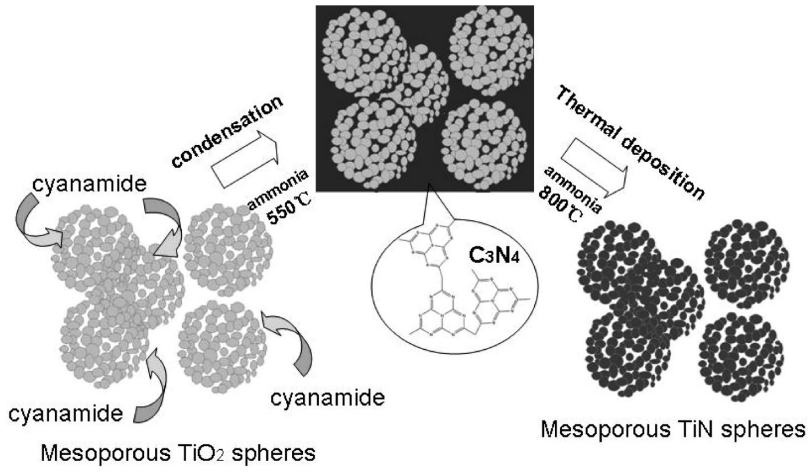


elemental composition of the resulting materials (Table 2). According to elemental analysis, traces of carbon can be detected. The amount of carbon residue is minor compared with that of previously reported TiN (4), TiN nanoparticles (31), and TiVN (ternary metal nitride) nanoparticles (37) using cyanamide or carbon nitride as the only nitrogen source. Furthermore, some oxygen element is also detected, which may result from surface oxidation as mentioned in

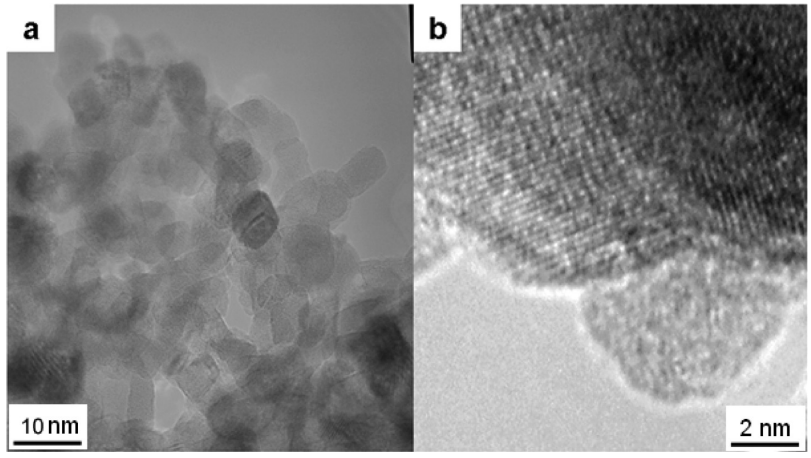


FIGURE 2. (a) TEM image and (b) HRTEM image of mesoporous TiN spheres with diameter range of 200−300 nm; (c) SAED pattern of the same TiN spheres.

**Table 2. Elemental Composition of the Mesoporous TiN Spheres with Different Diameter Ranges**

| materials | Ti% | N% | C% | O% |
|---|---|---|---|---|
| TiN-1 | 73.6 ± 2.0 | 16.5 ± 0.1 | 1.2 ± 0.3 | 7.2 ± 0.3 |
| TiN-2 | 69.5 ± 1.2 | 16.8 ± 0.1 | 0.7 ± 0.2 | 5.0 ± 0.1 |
| TiN-3 | 68.5 ± 0.8 | 15.9 ± 0.2 | 0.6 ± 0.1 | 6.2 ± 0.1 |

previous reports (35, 38). However, the present of TiN-TiO solid solution also can not be ruled out (further discussed in the next paragraph) (25).

Figure 3 shows that XRD patterns of the resultant black powders can be indexed to the typical pattern of the cubic TiN, belonging to the space group *Fm*3*m*. No peaks corresponding to rutile or anatase $TiO_2$ are observed in the XRD patterns. Therefore, the presence of large amount of titanium oxide can be excluded. However, the diffraction peaks shift to higher angles with the increasing size of mesoshperes, which indicates a decrease of lattice parameters. Indeed, the lattice parameters calculated from the three XRD patterns 4.20 Å ($a = b = c$), 4.19 Å, and 4.18 Å for TiN-1, TiN-2, and TiN-3, correspondingly. These results are smaller than that of TiN phase osbornite typical pattern (JCPDS 38−1420, 4.24 Å)[2] and previous reports by Kumta et al. (4.219 − 4,234 Å) (10) and Antonietti et al. (4.21 Å) (28). Accroding to Zukalova and Kavan et al. (25), it is ascribed to a partial formation of TiN-TiO solid solution and nonstoichiometric $TiN_x$. This result may be due to the incompletely nitridation of $TiO_2$ spheres with the increasing size. It is also worth noting that with decreasing spheres size, a progressively broadening of the diffraction peaks is observed in the samples. From [220] peak of XRD patterns, the average crystals size of TiN can be calculated to be approximately 2.9, 3.0, and 4.5 nm for TiN-1, TiN-2, and TiN-3, correspondingly, using the Scherrer equation.

The porosity of the TiN materials is determined by nitrogen sorption measurement (Figure 4 and Figure S3 in the Supporting Information). The $N_2$ adsorption−desorption isotherms of all materials are identified as Type IV isotherm indicating characteristics of mesoporous materials. Table 3 summarizes the surface areas, pore volumes, and average pore sizes determined from the BET isotherms. It can be seen that the surface area of TiN materials decrease from 92 to 56 $m^2\ g^{-1}$ with increasing size of the TiN spheres. The average pore sizes of Barrett−Joyner−Halenda (BJH) are

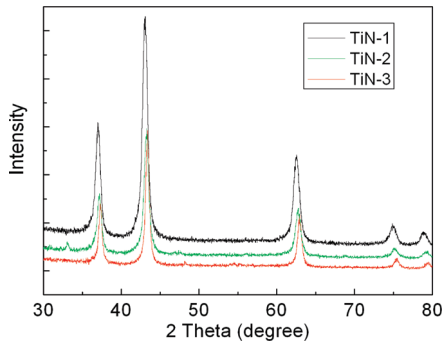


**FIGURE 3. XRD patterns of the mesoporous TiN spheres (black line refers to TiN-1, green line refers to TiN-2, red line refers to TiN-3).**

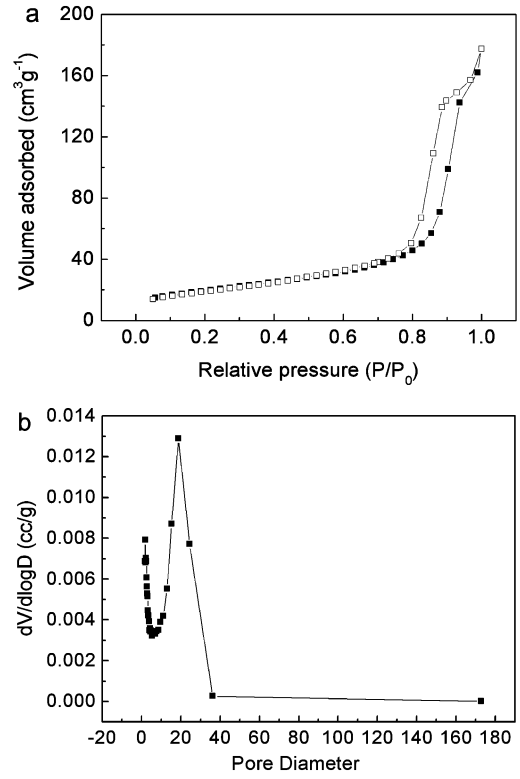


**FIGURE 4. (a) Nitrogen adsorption and desorption isotherms of mesoporous TiN micro- spheres TiN-2 and (b) their pore-size distribution obtained from adsorption branch of the isotherm using the BJH method.**

**Table 3. Porous Characteristics of the Mesoporous $TiO_2$ with Different Particle Sizes**

| materials | surface area $S_{BET}$ ($m^2\ g^{-1}$) | pore volume ($cm^3\ g^{-1}$) | pore size (nm) |
|---|---|---|---|
| TiN-1 | 92 | 0.57 | 27 |
| TiN-2 | 70 | 0.28 | 14 |
| TiN-3 | 56 | 0.29 | 20 |

obtained from the isotherm range from 14 to 27 nm, corresponding to TiN-2, TiN-3, and TiN-1, respectively. All these data strongly confirm the fact that the spheres have a mesoporous structure.

Cyclic voltammograms (CVs) tests were performed on mesoporous TiN spheres to evaluate their electrochemical performance for nonaqueous symmetric supercapacitors. As shown in Figure 5a, the CV curve is approximated to a rectangle which is reflective of an ideal capacitive behavior. Most of the capacity can be attributed to interface storage according to previous reports by J. Maier et al. (39−41). The specific capacitance of symmetric supercapacitor ($C$) is calculated according to the equation:

$$C = \frac{I\Delta t}{m\Delta V} \quad (1)$$

where $m$ is the total mass of the two electrodes, and $I$, $\Delta t$, and $\Delta V$ are the average current of charge and discharge, time and voltage, respectively. The single-electrode specific capacitance ($C_s$) can be calculate by the equation

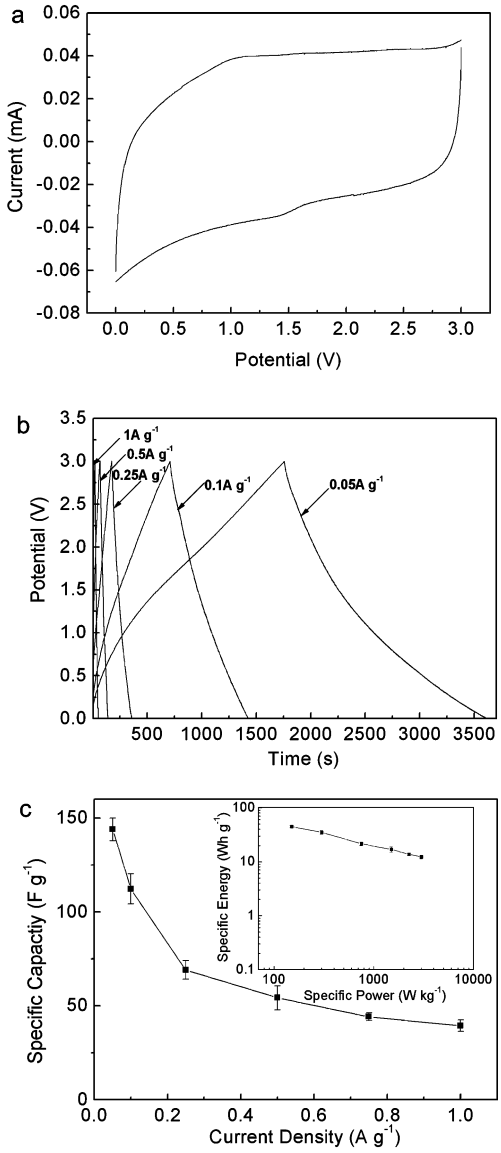


**FIGURE 5. (a) CV curve of TiN-2 cycled between 0 and 3 V at a sweep rate of 2 mV $s^{-1}$. (b) The charge/discharge curves of TiN-2 symmetric supercapacitor between voltage limits of 0−3.0 V at rates varied from 0.05A $g^{-1}$ to 1 A $g^{-1}$. (c) Single-electrode capacitance ($C_s$) of TiN-2 symmetric supercapacitor as a function of charge/discharge current density and the Ragone plot of TiN-2 symmetric supercapacitor (inset).**

$$\frac{1}{mC} = \frac{1}{m_s C_s} + \frac{1}{m_s C_s} \tag{2}$$

where $m_s$ is the mass of single electrode. Therefore, the single electrode $C_s$ of the TiN-2 is 133 F $g^{-1}$ at the scan rate of 2 mV $s^{-1}$.

Galvanostatic charge−discharge experiments were further carried out to test the mesoporous TiN spheres symmetric supercapacitors. The charge−discharge curves and cycling performance of TiN-2 supercapacitors under rates varied from 0.05 to 1 A $g^{-1}$ are shown in Figure 5b (the electrochemical performances of TiN-1 and TiN-3 supercapacitors are shown in the Figure S4, Supporting Information). The single electrode $C_s$ of the TiN-2 measured from galvanostatic charge−discharge tests can also be calculate by eq 1 when $I$ represents the current of discharge. Thus the $C_s$ of the TiN-2 are 144.0, 112.3, 69.1, 54.2, 44.2, and 39.4 F $g^{-1}$, corresponding to current densities of 0.05, 0.1, 0.25, 0.5, 0.75, and 1 A $g^{-1}$, respectively (Figure 5c). It should be noted that this result is a little higher than that obtained by the CV test, which is also in agreement with a previous work (42). Energy density and power density, as important parameters for the electrochemical performance of supercapacitor have been also presented for a detail evaluation of TiN materials. The power density and energy density can be calculated from the following equations (43)

$$E = \frac{1}{2}C(\Delta V)^2 \tag{3}$$

$$P = \frac{Q\Delta V}{2m\Delta t} = \frac{E}{t} \tag{4}$$

where $P$ (kW $kg^{-1}$), $C$ (F $g^{-1}$), $V$ (V), $Q$ (C), $m$ (kg), $\Delta t$ (s), and $E$ (W h $kg^{-1}$) are the power density, specific capacitance, potential window of discharge, charge delivered of discharge, mass of active materials, discharge time, and energy density, respectively. Ragone plot of TiN-2 (Figure 5c insert) showed that the energy densities reduce slightly with increasing power densities. The energy density of TiN-2 can reach 45.0 W h $kg^{-1}$ at a power density of 150 W$kg^{-1}$(based on the mass of active materials), and still remains 12.3 W h $kg^{-1}$ at a power density of 3 kW $kg^{-1}$, which indicate mesoporous TiN spheres are potential candidates for a high-energy supercapacitor.

## CONCLUSION

In summary, we have fabricated mesoporous titanium nitride spheres through a facile template free strategy. Using cyanamide as a structural confinement agent, $TiO_2$ mesoporous spheres were directly transformed into mesoporous TiN spheres at high temperature under an ammonia atmosphere. Through changing the amount of water during the procedure of preparing titanium glycolate spheres, mesoporous spheres with tunable diameters were obtained. It is also demonstrated that the mesoporous TiN spheres can serve as a promising electrode material for high energy supercapacitors. Furthermore, this mesoporous structure of TiN is potential framework for synthesizing composites with 3D mixed (electron and ion) conducting networks by introducing electroactive materials (e.g., $MnO_2$, $RuO_2$, Si, Sn) on the surface of mesoporous TiN spheres. Therefore, an excellent electrode material based on mixed conducting composites with a higher specific energy and power density can be expected, which is highly desirable for Li-ion batteries and supercapacitor applications.

**Acknowledgment.** The authors acknowledge the support by "100 Talents" program of the Chinese Academy of Sciences, and National Natural Science Foundation of China (Grants 20901044, 20971077, 20802039, and 20902052).

**Supporting Information Available:** SEM and TEM images of TiN prepared without the addition of cyanamide (Figure S1), low-magnification SEM images of the three mesoporous TiN spheres samples (Figure S2), nitrogen adsorption/desorption isotherms and the pore-size distribution of TiN-1 and TiN-3 (Figure S3), and electrochemical performance of TiN-1 and TiN-3 (Figure S4) (PDF). This material is available free of charge via the Internet at http://pubs.acs.org.

## REFERENCES AND NOTES


(1) Qiu, Y.; Gao, L. *J. Phys. Chem. B* **2005**, *109*, 19732.
(2) Drygas, M.; Czosnek, C.; Paine, R. T.; Janik, J. F. *Chem. Mater.* **2006**, *18*, 3122.
(3) Kaskel, S.; Schlichte, K.; Kratzke, T. *J. Mol. Catal. A: Chem.* **2004**, *208*, 291.
(4) Fischer, A.; Makowski, P.; Muller, J. O.; Antonietti, M.; Thomas, A.; Goettmann, F. *ChemSusChem* **2008**, *1*, 444.
(5) Yao, W.; Makowski, P.; Giordano, C.; Goettmann, F. *Chem.—Eur. J.* **2009**, *15*, 11999.
(6) Muhammed Musthafa, O. T.; Sampath, S. *Chem. Commun.* **2008**, *1*, 67.
(7) Kirchner, C. N.; Hallmeier, K. H.; Szargan, R.; Raschke, T.; Radehaus, C.; Wittstock, G. *Electroanalysis* **2007**, *19*, 1023.
(8) Wang, Y.; Yuan, H.; Lu, X.; Zhou, Z.; Xiao, D. *Electroanalysis* **2006**, *18*, 1493.
(9) Nakayama, T.; Wake, H.; Ozawa, K.; Kodama, H.; Nakamura, N.; Matsunaga, T. *Environ. Sci. Technol.* **1998**, *32*, 798.
(10) Choi, D.; Kumta, P. N. *J. Electrochem. Soc.* **2006**, *153*, A2298.
(11) Snyder, M. Q.; Trebukhova, S. A.; Ravdel, B.; Wheeler, M. C.; DiCarlo, J.; Tripp, C. P.; DeSisto, W. J. *J. Power Sources* **2007**, *165*, 379.
(12) Yuan, Z.-Y.; Su, B.-L. *J. Mater. Chem.* **2006**, *16*, 663.
(13) Wan, Y.; Shi, Y.; Zhao, D. *Chem. Commun.* **2007**, *1*, 897.
(14) Yang, P.; Deng, T.; Zhao, D.; Feng, P.; Pine, D.; Chmelka, B. F.; Whitesides, G. M.; Stucky, G. D. *Science* **1998**, *282*, 2244.
(15) Holland, B. T.; Abrams, L.; Stein, A. *J. Am. Chem. Soc.* **1999**, *121*, 4308.
(16) Kanatzidis, M. G. *Adv. Mater.* **2007**, *19*, 1165.
(17) Boettcher, S. W.; Fan, J.; Tsung, C.-K.; Shi, Q.; Stucky, G. D. *Acc. Chem. Res.* **2007**, *40*, 784.
(18) Guo, Y.; Hu, Y.; Sigle, W.; Maier, J. *Adv. Mater.* **2007**, *19*, 2087.
(19) Davis, M. E. *Nature* **2002**, *417*, 813.
(20) Mazumder, B.; Hector, A. L. *J. Mater. Chem.* **2009**, *19*, 4673.
(21) Buha, J.; Djerdj, I.; Antonietti, M.; Niederberger, M. *Chem. Mater.* **2007**, *19*, 3499.
(22) Chen, H. Y.; Nambu, A.; Wen, W.; Graciani, J.; Zhong, Z.; Hanson, J. C.; Fujita, E.; Rodriguez, J. A. *J. Phys. Chem. C* **2007**, *111*, 1366.
(23) Jiang, Q. W.; Li, G. R.; Gao, X. P. *Chem. Commun.* **2009**, 6720.
(24) Jacob, K. T.; Verman, R.; Mallya, R. M. *J. Mater. Sci.* **2002**, *37*, 4465.
(25) Zukalova, M.; Prochazka, J.; Bastl, Z.; Duchoslav, J.; Rubacek, L.; Havlicek, D.; Kavan, L. *Chem. Mater.* **2010**, *22*, 4045.
(26) Worsley, M. A.; Kuntz, J. D.; Cervantes, O.; Han, T. Y.; Gash, A. E.; Satcher, J. H.; Baumann, T. F. *J. Mater. Chem.* **2009**, *19*, 7146.
(27) Li, J.; Gao, L.; Sun, J.; Zhang, Q.; Guo, J.; Yan, D. *J. Am. Ceram. Soc.* **2001**, *84*, 3045.
(28) Jun, Y.; Hong, W. H.; Antonietti, M.; Thomas, A. *Adv. Mater.* **2009**, *21*, 4270.
(29) Gray, B. M.; Hassan, S.; Hector, A. L.; Kalaji, A.; Mazumder, B. *Chem. Mater.* **2009**, *21*, 4210.
(30) Yu, T.; Deng, Y.; Wang, L.; Liu, R.; Zhang, L.; Tu, B.; Zhao, D. *Adv. Mater.* **2007**, *19*, 2301.
(31) Fischer, A.; Antonietti, M.; Thomas, A. *Adv. Mater.* **2007**, *19*, 264.
(32) Fischer, A.; Jun, Y.; Thomas, A.; Antonietti, M. *Chem. Mater.* **2008**, *20*, 7383.
(33) Bang, K.; Suslick, S. *Adv. Mater.* **2009**, *21*, 3186.
(34) Ren, Y.; Hardwick, L. J.; Bruce, P. G. *Angew. Chem., Int. Ed.* **2010**, *49*, 2570.
(35) Yu, Y.; Gu, L.; Zhu, C.; Tsukimoto, S.; van Aken, P. A.; Maier, J. *Adv. Mater.* **2010**, *22*, 2247.
(36) Zhong, L.-S.; Hu, J.-S.; Wan, L.-J.; Song, W.-G. *Chem. Commun.* **2008**, *10*, 1184.
(37) Jiang, X.; Herricks, T.; Xia, Y. *Adv. Mater.* **2003**, *15*, 1205.
(38) Fischer, A.; Muller, J. O.; Antonietti, M.; Thomas, A. *ACS Nano* **2008**, *12*, 2489.
(39) Maier, J. *Nat. Mater.* **2005**, *4*, 805.
(40) Balaya, P.; Li, H.; Kienie, L.; Maier, J. *Adv. Mater.* **2006**, *18*, 1421.
(41) Jamnik, J.; Maier, J. *Phys. Chem. Chem. Phys.* **2003**, *5*, 5215.
(42) Pang, S. C.; Anderson, M. A.; Chapmanb, T. W. *J. Electrochem. Soc.* **2000**, *147*, 444–450.
(43) Zolfaghari, A.; Ataherian, F.; Ghaemi, M.; Gholami, A. *Electrochim. Acta* **2007**, *52*, 2806.


AM100951H